

Electricity Generation and Self-Powered Sensing Enabled by Dynamic Electric Double Layer at Hydrogel–Dielectric Elastomer Interfaces

Luyao Jia, Zi Hao Guo, Longwei Li, Chongxiang Pan, Panpan Zhang, Fan Xu, Xiong Pu,* and Zhong Lin Wang*

Cite This: <https://doi.org/10.1021/acsnano.1c06950>

Read Online

ACCESS |

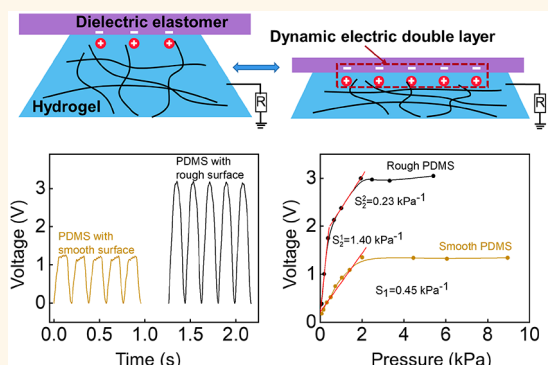
Metrics & More

Article Recommendations

Supporting Information

ABSTRACT: The electric double layer (EDL) at liquid–solid interfaces is fundamental to many research areas ranging from electrochemistry and microfluidics to colloidal chemistry. Here, we demonstrate the electricity generation by mechanically modulating the EDL at the hydrogel–dielectric polymer interfaces. It is found that contact electrification between the hydrogel and the dielectric polymer could charge the dielectric polymer surface at first; the mechanical deformation of the pyramid-shaped hydrogel results in the periodic variation of the EDL area and capacitance, which then induces an alternative current in the external circuits. This mechano-to-electrical energy conversion mechanism is then utilized to construct soft stretchable self-powered pressure sensors by designing dynamic EDL at hydrogel–dielectric elastomer interfaces. The sensitivity is optimized to 1.40 kPa^{-1} in the low-pressure range of 31–300 Pa by increasing the elastomer roughness. Its antifreeze performance is also improved by adding ethylene glycol into the hydrogel. The capability in detecting subtle human activities is further demonstrated. This mechano-electrical energy conversion and the corresponding self-powered sensor can be widely applied in future soft electronics.

KEYWORDS: electric double layer, electricity generation, triboelectric nanogenerator, self-powered sensor, stretchable electronics



INTRODUCTION

The electric double layer (EDL) is widely known to describe the interaction between ions and solid surfaces at the liquid/solid interfaces, which lays the foundation of many research areas such as electrochemistry, microfluidics, and colloidal chemistry.^{1–4} Recent studies have shown that modulating the EDL at liquid/solid interfaces with different environmental stimuli can lead to electricity generation, including kinetically induced variation of liquid/solid interfaces,^{5–8} thermal evaporation of water,^{9,10} and humidity variations.^{11–13} In particular, a number of studies have found that electricity can be generated by different kinetic motions (dropping, waving, or flowing) of water or water droplets on various solid surfaces, including dielectric polymers,^{5,8,14–17} inorganic oxides,^{18–20} and carbon nanomaterials.^{21–23} These different mechanical stimuli can change the EDL capacitance or increase the interface charge quantities, leading to the potential differences and electrical current between the two electrodes. For example, the high-voltage

triboelectric nanogenerators (TENG) were reported by striking water droplets or waving bulk water on the hydrophobic polymer surfaces.^{7,8} Similarly, electricity generation was reported by squeezing a water droplet placed between an electrode and a polymer-coated electrode.^{15,17} Electricity generation was also achieved by dropping or waving water on carbon nanomaterials.^{21,22}

The wide investigations of these dynamic EDL-based electricity generators also draw interest to the mechanism on the origin of surface charges at the liquid/solid interfaces. Even though the Gouy–Chapman–Stern model¹ has been well-

Received: August 12, 2021

Accepted: December 8, 2021

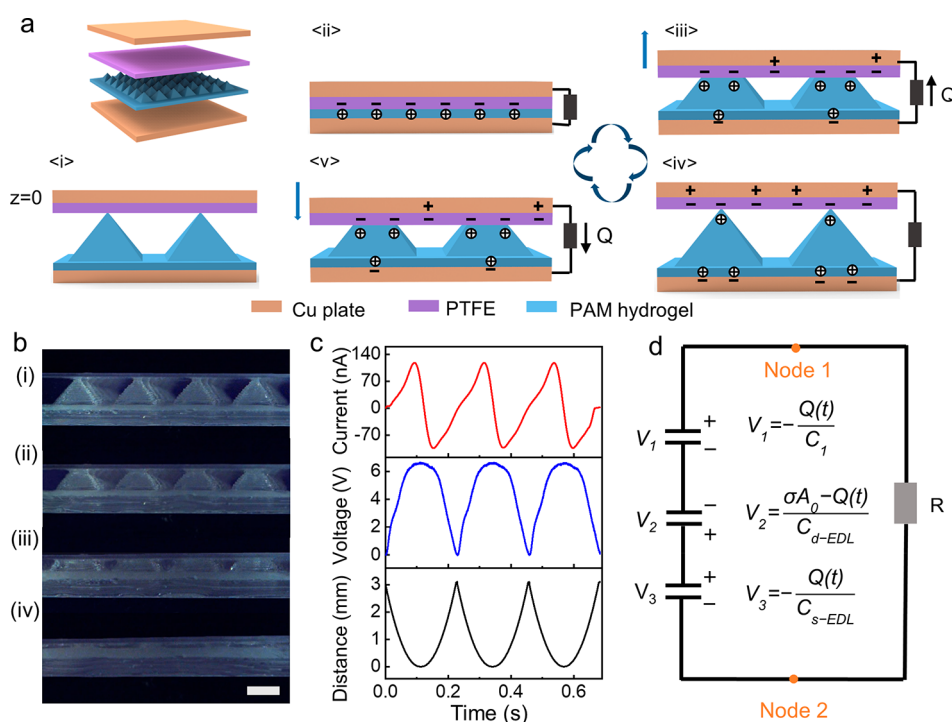


Figure 1. Electricity generation by dynamic EDL at hydrogel–dielectric polymer interfaces. (a) Scheme of the structure and working mechanism of the dynamic EDL-based TENG with pyramid-shaped hydrogel. (b) Photographs showing the process of squeezing the pyramid hydrogel (scale bar: 3 mm). (c) Short-circuit current, open-circuit voltage of the pyramid TENG and the moving distance of the upper dielectric layer. The traveling distance of the upper dielectric layer (z) is zero when it contacts the tips of hydrogel pyramids before pressing. (d) Equivalent circuit model of the dynamic EDL-based TENG.

established to theoretically describe the structure and the potential drop of the EDL, the origin of the surface charges is still not clearly and comprehensively understood.^{5,24} Recent studies have found that the contact electrification involved with the electron transfer process at the liquid/solid interfaces contributes to the formation of charged solid surfaces, different from various traditional mechanisms such as ionization, dissolution, or ion adsorption of the solid surfaces.^{5,18,20,24,25} Then, Wang's hybrid EDL model was proposed to describe the two-step formation process of the EDL, based on contact electrification and subsequent electrostatic counterion adsorption.^{20,26} It is nevertheless noted that there is still argument about the charge transfer mechanism of contact electrification at the solid–liquid interfaces.^{27,28}

Despite this progress, study is still rare for utilizing hydrogel electrolyte to construct dynamic EDL. The hydrogel is in solid form, which will certainly extend the applications of these electricity generation devices.^{29–31} Thus, the mechano-electrical conversion by dynamic EDL can potentially be applied for designing self-powered force-sensitive sensors. Compared with the intensively reported resistive or capacitive pressure/strain sensors, the self-powered sensing unit requires no electricity sources, since it directly outputs electrical signals in response to the mechanical stimuli.^{32–34}

Therefore, we demonstrated herein the electricity generation by a mechanical motion-induced dynamic EDL at the hydrogel–dielectric elastomer interfaces, and showed its application as a self-powered soft pressure sensor for monitoring human activities. By varying the interface areas, the EDL capacitance changes, and the unbalanced charges on elastomer surfaces induce alternative current in external circuits. Furthermore, the sensitivity of electrical outputs responsive to the mechanical

pressure was optimized by increasing interface roughness, reaching 1.40 kPa^{-1} in the low pressure range of 31–300 Pa. Due to the high sensitivity, softness, and stretchability of the self-powered sensor, its capability in detecting subtle human activities was demonstrated, such as throat movements, vocal cord vibrations, muscle motions, and abdominal breathing.

RESULTS AND DISCUSSION

We first constructed a dynamic interface between a hydrogel film (polyacrylamide, PAM) and a dielectric polymer (polytetrafluoro ethylene, PTFE). To design an electricity generation device based on dynamic EDL, the PAM hydrogel with pyramid arrays was placed between a Cu plate and another PTFE-coated Cu plate (Figure 1a). We define that the traveling distance of the top plate (z) is zero when it contacts the tips of hydrogel pyramids before pressing (Figure 1a <i>); z reaches maximum (z_{max}) when the PTFE is fully covered by hydrogel (Figure 1a <ii>). As demonstrated previously that the contact electrification between water and dielectric polymers can charge the solid surfaces with static charges,^{5,20,24} this applies here as well, since the hydrogel is swollen with about 80 wt % deionized water. As the contact electrification contributes to the formation of charged PTFE surfaces, this device is termed a triboelectric nanogenerator (TENG).³⁵ As the PTFE is highly tribo-negative, it is negatively charged after the electrification. The charged PTFE surface will attract counterions in the water to form an EDL by the Coulombic force. When the pressure is released and the top PTFE-coated Cu plate moves upward, the unscreened charges on the PTFE surfaces will induce the formation of opposite charges in the upper Cu electrode, leading to the electrical current from the downside to the upper Cu electrode (Figure 1a <iii>). The current stops when the upper electrode

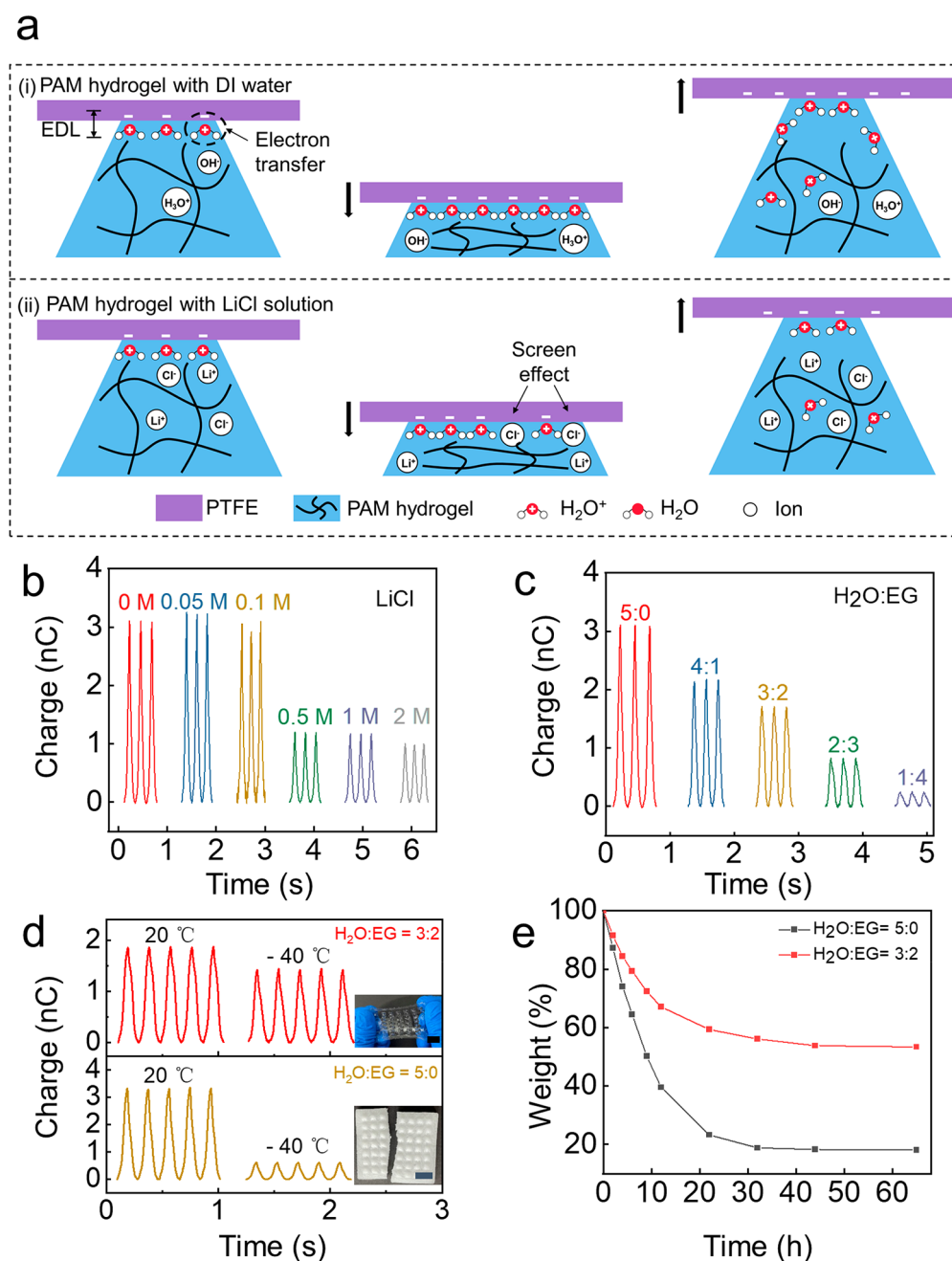


Figure 2. Contact electrification mechanism and optimization between the hydrogel and dielectric polymers. (a) Mechanism of contact electrification: (i) between pyramid hydrogel with deionized water and PTFE, and (ii) between pyramid hydrogel containing LiCl solution and PTFE. The transferred short-circuit charges when using (b) the hydrogel containing different concentrations of LiCl solution and (c) water–EG mixture solutions with different volume ratios. (d) Comparison of the transferred short-circuit charges at low temperature when using hydrogel with deionized water or water–EG mixture. The insets are photos of the two hydrogels frozen at $-40\text{ }^{\circ}\text{C}$ for 3 h (scale bar: 3 cm). (e) Water retention percentage of these two hydrogels at room temperature.

returns to the position $z = 0$ (Figure 1a <iv>), but a reversed current flow occurs when pressing the device again (Figure 1a <v>). Figure 1b recorded the cross-sectional photos of the device when pressing it. The deformation of the hydrogel and the increase of the hydrogel–PTFE interface area were clearly observed during the pressing process. The EDL capacitance at the interface between the hydrogel and PTFE varies with the change of the contact area between the hydrogel and PTFE by the mechanical motion. The output generation here is different from the streaming current/potential. According to the previous reports, streaming current is generated by the transportation of

counterions in EDL along with the solution flowing under the pressure gradient, which is also associated with the change of EDL.³⁶ The streaming current converts hydrostatic energy to electrical power by the pressure-driven transport of ions in the EDL. This work generates electricity by changing the EDL capacitance through mechanical motion. This electricity generation process had been previously reported by several studies.^{15,37} However, the PTFE layer was previously neglected when considering the mechanically modulated EDL. Since the EDL exists at the solid–electrolyte interfaces in direct contact and is in the nanometer thickness range, the thick PTFE ($70\text{ }\mu\text{m}$

in our work and 300 nm in a previous work¹⁵) should be considered. Then, the dynamic EDL should be located at the PTFE–hydrogel interface, and the formation of this EDL involves the electrification process as well.

The typical short-circuit current (I_{sc}) and open-circuit voltage (V_{oc}) are shown in Figure 1c. The amplitude of I_{sc} reaches 115 nA, and the maximum V_{oc} is 6.5 V for a hydrogel film with pyramid height of 3 mm and pyramid number of 7×7 (total area is $4 \times 4 \text{ cm}^2$). We further optimized the height of the hydrogel pyramid, with the bottom side length fixed at 4 mm. The Q_{sc} increased first with the height and then showed less variation after reaching 3 mm height (Figure S2). By fixing the pyramid size, the output improved with the pyramid number due to the increased total device area. Therefore, we fixed the pyramid height and number to 3 mm and 7×7 for all following tests, other than mentioned specifically.

The dynamic EDL-based TENG can be equivalent to a circuit consisting of a series of capacitors, as depicted in Figure 1d. The top electrode and the charged PTFE surfaces can be represented as the capacitor C_1 ; the EDL capacitor at the PTFE–hydrogel interface varying with the mechanical motion is termed C_{d-EDL} ; whereas the capacitance of the EDL at the hydrogel–bottom electrode interface is approximately steady and termed C_{s-EDL} . As the mechanical motion breaks the charge equilibrium in the dynamic EDL capacitor, there will be induced charges in the top and bottom electrodes with quantity of $Q(t)$. At the short-circuit condition, the voltage between the top and bottom electrode will be zero; while at open-circuit condition, the total transferred charge quantity is zero. Then, the V_{oc} , Q_{sc} , and I_{sc} can be derived as

$$V_{oc} = \sigma A_0 \frac{\lambda_d}{\epsilon_0 \epsilon_h A(t)} \quad (1)$$

$$Q_{sc} = \frac{\sigma A_0 \lambda_d}{C \epsilon_0 \epsilon_h A(t) + \lambda_d} \quad (2)$$

$$I_{sc} = \frac{dQ_{sc}}{dt} = \frac{C \epsilon_0 \epsilon_h \sigma A_0 \lambda_d}{(C \epsilon_0 \epsilon_h A(t) + \lambda_d)^2} \frac{dA(t)}{dt} \quad (3)$$

where ϵ_0 is vacuum permittivity, ϵ_h is the dielectric constant of the hydrogel, λ_d is the thickness of the top EDL, $A(t)$ is the varying hydrogel–PTFE interface area, and A_0 is the area of the charged PTFE surface area or the maximum hydrogel–PTFE interface area. C is a constant written as $C = \frac{1}{C_1} + \frac{1}{C_{s-EDL}}$. The detailed derivation can be seen in the Figure S3 and Supporting Information Note 1. It can be seen that V_{oc} is inversely proportional to the hydrogel–PTFE interface area $A(t)$; the I_{sc} is alternative when pressing and releasing the top electrode alternately. These trends are consistent with the experimental data as depicted in Figure 1c. The power output density of the dynamic EDL-based TENG was measured by connecting it in series with various load resistances arranging from 10 K Ω to 100 M Ω . The maximum power density of 1 mW/m² was obtained at a matched resistance of 4 M Ω (Figure S4). Meanwhile, the output–frequency relationship of the dynamic EDL-based TENG was studied, as shown in Figure S5. The V_{oc} of the TENG remains almost invariable with the frequency ranging 1–10 Hz.

This dynamic EDL-based TENG is also suitable to study the electrification behavior at the hydrogel–dielectric polymer interfaces, as the electrical outputs are positively proportional

to the generated charge density in the PTFE surfaces (σ) according to eqs 1–3. First, we compared the devices using PAM hydrogels swollen with DI water and LiCl solutions, respectively (as schematically shown in Figure 2a). It can be seen that the transferred charge quantity Q_{sc} sustains little variation (3.1–3.25 nC) when adding a trace amount of salt in the hydrogel (<0.1 M LiCl), but it decreases dramatically to ~ 0.97 nC when the LiCl concentration is higher than 0.5 M (Figure 2b). Coincidentally, the transferred charge quantity Q_{sc} has a similar changing pattern when different concentrations of NaCl are added into the hydrogel, as shown in Figure S6. At the same concentration of 0.05 mol/L, the charge quantity reaches the maximum value. This trend is consistent with a previous study using droplets of deionized water or salt solution.^{18,24} It can be explained schematically as Figure 2a. Despite the dispute on charge transfer mechanism in contact electrification,^{27,28} we adopted an electron transfer mechanism to explain this result, since the electrified charge quantity is high when using the hydrogel with deionized water. As suggested previously,^{5,24,38} the electron transfers between water molecule and the PTFE contribute to the electrified charges. Meanwhile, H_2O^+ will be generated during the contact electrification process. When the electron of a water molecular transfers to PTFE surfaces, it becomes cationic H_2O^+ . The lifetime of H_2O^+ is proven to be less than 50 fs, and it joins with a neighboring water molecule to yield an OH radical and H_3O^+ based on the reaction $\text{H}_2\text{O}^+ + \text{H}_2\text{O} \rightarrow \text{OH}\cdot + \text{H}_3\text{O}^+$.³⁹ In the actual case, H_3O^+ should form the EDL with the charged PTFE surface, as the lifetime of H_2O^+ is short. Nevertheless, H_2O^+ is illustrated in the EDL structure in Figure 2a to better show the electrification process. When adding an excess amount of salt in the hydrogel, there will be a large number of free ions in the hydrogel, which can screen the interface from the electron transfer process between a water molecule and the PTFE. Therefore, the contact electrification is suppressed if the salt concentration is higher than a certain value. The reduced electrified charges on PTFE surfaces account for the lower electrical outputs of the devices using hydrogels swollen with concentrated salt solutions. Previously, we reported TENGs with hydrogel or other solid-state ionic conductors as the electrode.^{40,41} We found that the salt concentration had a negligible impact on the performances,⁴⁰ and high outputs can still be obtained even when the conductivity is as low as 10^{-6} S/cm. This may be because the transferred charge quantity is low and the ion-migrating process is not the bottleneck step. In this study, the hydrogel functions both as an electrification layer and an ion-migrating electrode. In contrast, it is concluded that the salt addition is detrimental to the performances.

We also studied the interface electrification when adding ethylene glycol (EG) in the hydrogel. The transferred charge quantity Q_{sc} decreases with the decrease of the water-to-EG volume ratio (Figure 2c). Compared to the hydrogel with only deionized water, the Q_{sc} decreases from 3.1 nC to 2.17 nC, 1.7 nC, 0.81 nC, and 0.28 nC, when the water-to-EG ratio is 4:1, 3:2, 2:3, and 1:4, respectively. This trend can be attributed to the smaller polarity of EG than water. Despite the reduced contact electrification at the hydrogel–PTFE interface, the two following beneficial effects are obtained using the water–EG mixture in the hydrogel. First, the EG is commercially used as an antifreeze agent, which can reduce the freezing point of the mixture, thereby widening the operation temperature range of the device.⁴² Typically, the mixture has the best antifreeze properties with an EG volume percentage around ~ 40 –60%.⁴³

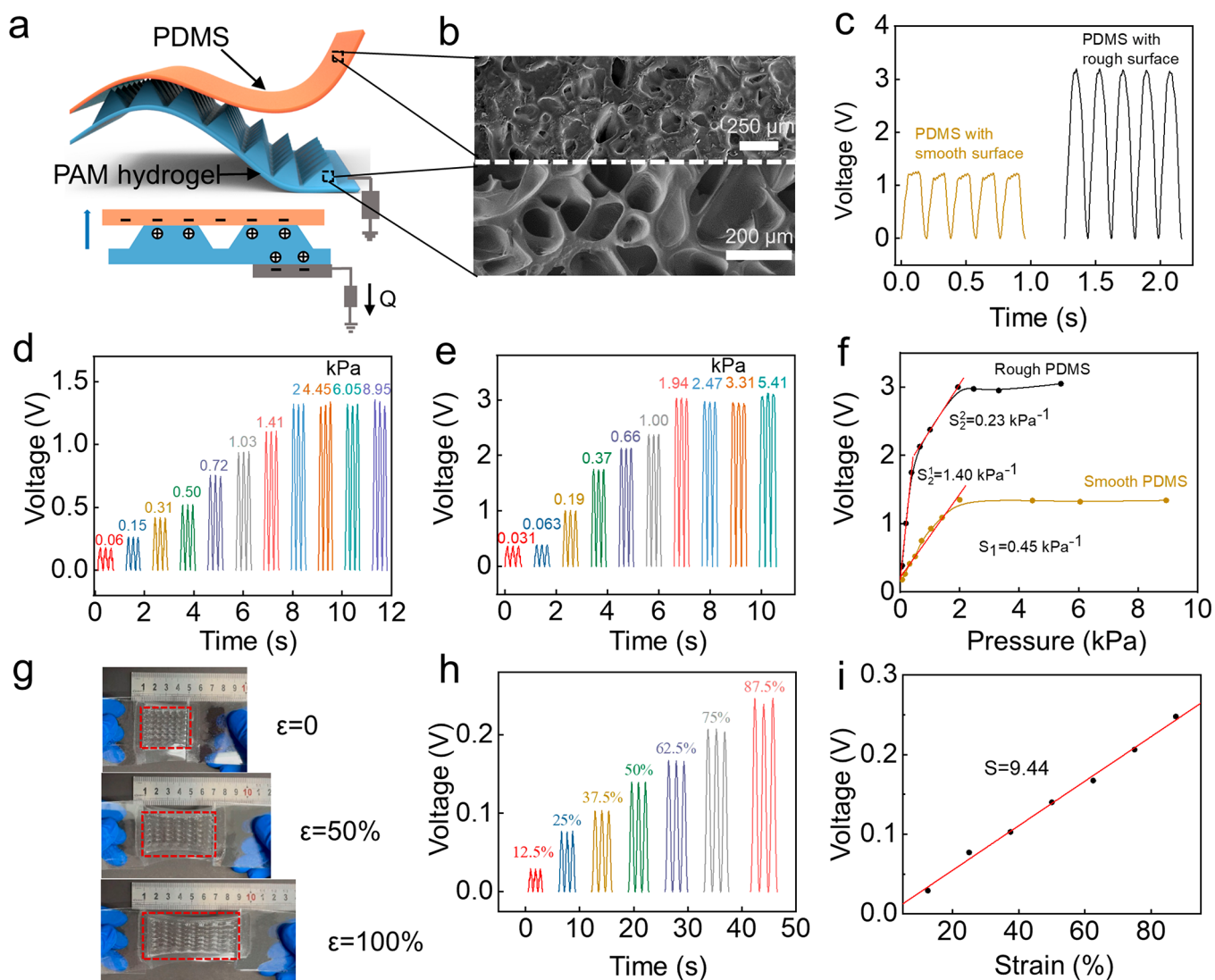


Figure 3. Self-powered soft sensor. (a) Schematic illustration of single-electrode TENG sensor based on the dynamic EDL at hydrogel–elastomer interfaces (upper). EDL formed at the PDMS/hydrogel interface and the metal wire/hydrogel interface, respectively (lower). (b). SEM images of the PDMS with rough surface (upper) and SEM images of the hydrogel being lyophilized (lower). (c) Comparison of the voltage of the TENG sensor using PDMS with smooth and rough surface. Comparison of the voltages of these two sensors under a series of pressure stimuli: (d) smooth PDMS and (e) rough PDMS. (f) Summarized voltage–pressure variation of these two sensors and their corresponding sensitivities. (g) Photos of the sensor at initial state and different stretched states. (h) Voltage of the TENG sensor by stretching to different strains. (i) Summarized voltage–strain variation and sensitivity.

Therefore, the water-to-EG ratio was selected as 3:2 for the hydrogel. After being frozen at $-40\text{ }^{\circ}\text{C}$ for 3 h, the Q_{sc} of the device using a water–EG mixture can still be 1.4 nC, showing a limited decrease compared to that operating at $20\text{ }^{\circ}\text{C}$, whereas the Q_{sc} of the device using hydrogel with water only can just be 0.58 nC, only about 1/5 of that operating at $20\text{ }^{\circ}\text{C}$ (Figure 2d). As shown by the inset photos in Figure 2d, the hydrogel with EG is still able to be stretched, but the hydrogel containing water only is completely frozen and brittle after freezing at $-40\text{ }^{\circ}\text{C}$ for 3 h. Second, the EG has a much higher boiling point and is nonvolatile compared with water, which helps to improve the environmental stability of the device. The open-circuit voltage of the samples above has the same trend as the Q_{sc} , as shown in Figure S7. When storing at a temperature of $25\text{ }^{\circ}\text{C}$ and relative humidity of 17%, the hydrogel containing water only was almost completely dehydrated after 30 h; while the hydrogel with the water–EG mixture retained a stable weight retention rate of

about 60% after 60 h (Figure 2e). When tested in air without encapsulation, the water in the hydrogel still evaporate which cause that the V_{oc} of the TENG declines after dehydration for 24 h and then maintains stable (Figure S8). Appropriate encapsulation is required for future practical applications.

After these mechanism and optimization studies, we designed a soft and stretchable self-powered pressure/strain sensor based on the dynamic EDL-based TENG. Traveling distance of the top electrode will increase with the pressure, which will lead to the larger maximum interface area for contact electrification and thereby higher V_{oc} . This pressure-sensitive outputs make it potentially viable for pressure sensors. In order to achieve the softness and stretchability, the sensor was designed as schematically shown in Figure 3a. A single-electrode structure was adopted and a dielectric elastomer (polydimethylsiloxane, PDMS) was selected for replacing the unstretchable PTFE. Meantime, PAM hydrogel with water-to-EG ratio of 3:2 was

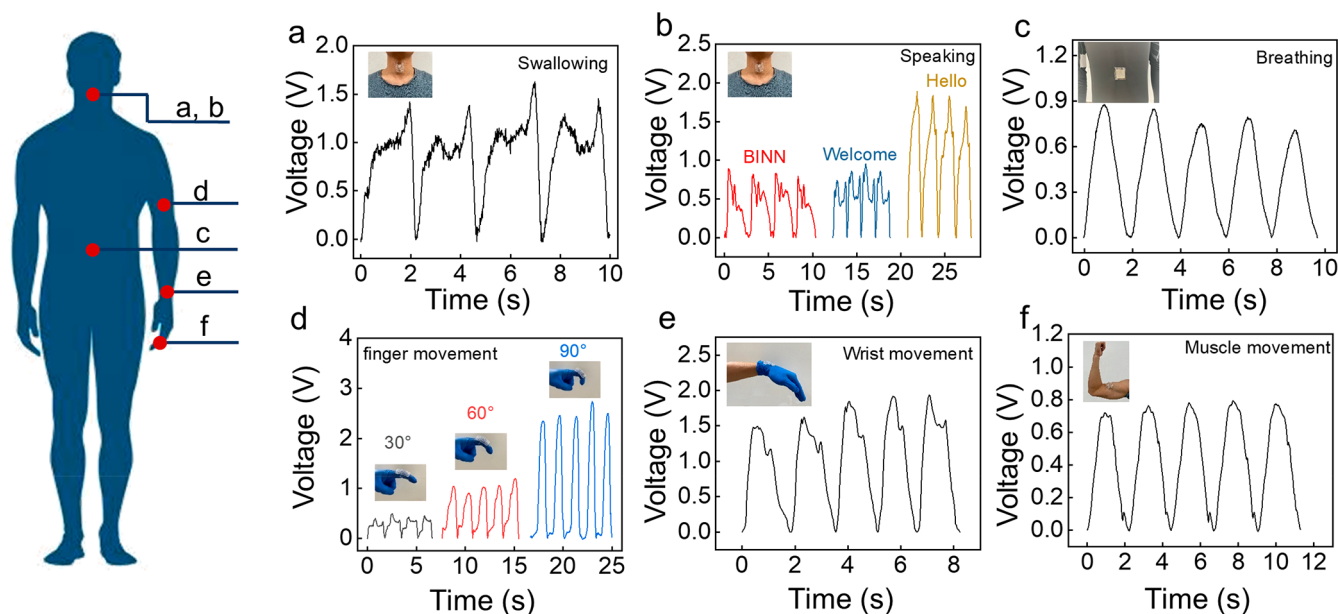


Figure 4. Demonstration of the self-powered sensor for detecting subtle mechanical motions. The sensor is attached to the throat for (a) swallowing and (b) speaking detection; and (c) breathing detection by attaching it on the belly. (d,e) Signals of human joint motion from the fingers and wrist. (f) Voltage of the sensor induced by the muscle movement.

selected, considering the combined performances of high output, antifreeze, and antidehydration capabilities. The ionic conductivity of the PAM hydrogel with water-to-EG ratio of 3:2 is $1.31 \times 10^{-3} \text{ S/cm}$ at the room temperature (Figure S9). The thickness of the PDMS was optimized to be about $200 \mu\text{m}$ (Figure S10). The total area of the device is $4 \times 4 \text{ cm}^2$; the size of the hydrogel pyramid is $4 \text{ mm} \times 4 \text{ mm} \times 3 \text{ mm}$; the pyramid number is 7×7 . Considering that the sensitivity of the sensor can be improved by increasing the roughness of the hydrogel–PDMS interfaces, we further introduce rough microstructures to the PDMS by using sandpaper (roughness of no. 180 #) as the casting mold. The top surface of the hydrogel pyramid forms dynamic EDL together with the PDMS, while the bottom hydrogel surface forms static EDL together with a metal wire, as shown in the bottom picture of Figure 3a. The small metal wire–hydrogel interface here ensures the stretchability of the whole device. The whole electricity generation process of the device is illustrated in Figure S11. The selected PDMS surface contacting the hydrogel pyramid possesses a rough surface with protrusions and grooves at micrometer scale, as shown in the top SEM image of Figure 3b. The bottom SEM photo of Figure 3b shows the morphology of the hydrogel after being lyophilized. In order to measuring the open-circuit of the sensor, the PDMS and the hydrogel both are adhered to the tough acrylic plate due to the softness. Then, the output performance of the TENG sensor is measured by pressing the pyramid tip of the hydrogel with PDMS using a step motor. Compared with the device using a smooth PDMS surface (V_{oc} is 1.21 V), the V_{oc} of the device using rough PDMS reaches approximately 3.19 V (Figure 3c). This confirms that the rougher interface effectively enhances the output property, which is attributed to the increase in the effective contact area at the interface for electrification.⁴⁴ Then, the V_{oc} of the device was measured at different frequencies ranging 1–10 Hz (Figure S12). The electrical output of the sensor remains invariant under wide frequency, which can ensure the reliable monitoring for human motion with variable frequency. Besides, the sensor also exhibits excellent durability even after 6000 cycles (Figure S13).

To determine the sensitivity of the pressure sensor, the V_{oc} values of the two devices with smooth and rough PDMS were recorded under diverse pressures, respectively (Figure 3d and e). The V_{oc} increases linearly with the pressure and reaches saturation when the pressure is higher than about 2 kPa. Therefore, the sensitive pressure range of the sensor was estimated to be 0.063–2 kPa and from 0.031–1.938 kPa for device with smooth and rough PDMS, respectively. The sensitivity (S) can be calculated by

$$S = (d\Delta V/V_s)/dP \quad (4)$$

where ΔV represents the relative change of the open-circuit voltage, V_s is the saturated voltage, and P denotes the pressure. The sensitivity of the device with smooth PDMS is calculated to be 0.45 kPa^{-1} before the pressure reaches 2 kPa, whereas the sensitivity of the sensor with rough PDMS is calculated to be 1.40 kPa^{-1} as the pressure is below 0.3 kPa, and 0.23 kPa^{-1} within the pressure range of 0.3–2 kPa (Figure 3f). The higher sensitivity at low pressure of the device with rough PDMS is attributed to the deformation of PDMS microstructures at low pressure, which leads to the larger change in the interface area and thereby higher voltage variation comparing with that using smooth PDMS.^{44,45} When the pressure increased higher than 2 kPa, complete deformation of the pyramid was achieved, and then the voltage did not further increase with the pressure. Moreover, Figure S14 indicates that the response time of our sensor is about 26 ms under the load of 1 kg. It is noted that the sensitivity or pressure range of the sensor may be improved by tuning the elastic modulus of the hydrogel in the future work as indicated by previous reports.^{46,47}

Due to the stretchability of both the PDMS and hydrogel, the self-powered sensor is stretchable. Because of the pyramid structure, the stretchability of the hydrogel decreased, exhibiting a fracture strain of 142% (Figure S15). As shown by photos in Figure 3g, it can be uniaxially stretched to elongation ratio of $\lambda = 2$ ($\epsilon = 100\%$ strain) without failure. It can also be twisted at diverse torsion angles, as shown in Figure S16. We found that the

dynamical EDL-based TENG sensor can also output electrical signals at tensile stretching deformation. As the device is stretched gradually to larger strain ($\epsilon = 12.5\%$, 25% , 37.5% , 50% , 62.5% , 75% , and 87.5%), the corresponding open-circuit voltages increase accordingly ($V_{oc} = 0.029$, 0.076 , 0.103 , 0.139 , 0.167 , 0.210 , and 0.250 V, respectively), as shown in Figure 3h. This implies that the hydrogel–PDMS interface area also changes with the tensile deformation, leading to the deformation-induced dynamical EDL at the interfaces and the electrical outputs. The voltage changes approximately with the tensile strain (Figure 3i). The sensitivity to the strain can be given by

$$S = (d\Delta V/V_0)/d\epsilon \quad (5)$$

where ΔV represents the relative change of the open-circuit voltage, V_0 is the minimum voltage, and ϵ denotes the strain. The sensitivity of the SF-TENG sensor is 9.44 in the strain range from 12.5% to 100%. Moreover, when the sensor is placed at different temperatures (-40 to 80 °C), the output voltage peak value remains quite stable at the temperature range of -20 to 40 °C (Figure S17), which means that the sensor can be used at a relatively wide temperature range.

Due to the high sensitivity of the TENG sensor to pressing and stretching deformation, it can be used to monitor diverse human activities, including throat movements, vocal cord vibrations, abdominal breathing, joint and muscle movements, and so on. The optimized TENG sensor was attached to different parts of the human body by the adhesive tape, and the voltages were measured in real time of the human activities. Compared with other traditional iontronic pressure sensors,^{48,49} the voltage of our sensor can be directly measured without a power source device. The power consumption of our device is lower than that of resistive or capacitive pressure/strain sensors. By attaching the device on the neck, the voltage waveform can distinguish the subtle mechanical motions of the throat when swallowing and speaking, as shown by Figure 4a,b and Video S1, respectively. When speaking different words, the corresponding voltages of the sensor show different waveforms and peak values, whereas the voltages have the same waveforms when repeating the same word multiple times (Figure 4b), which makes it possibly viable for biometric applications or voice-machine interaction. Then, the sensor was attached to the abdominal wall to monitor deep breathing of human bodies (Figure 4c, Video S1). The periodic breathing of the human body can be clearly observed from the voltage waveforms, which means it is also possible to help monitor a person with apnea syndrome. Furthermore, the sensor was also able to monitor stronger mechanical deformations caused by joint and muscle movements, such as finger and wrist flexion, biceps brachii movement, knee and elbow movement, as shown in Figure 4d,e,f and Figure S18, respectively. As the finger was bent at various angles (30° , 60° , 90°), the peak values of voltages gradually increase, making it also possible for application such as human–machine interaction. Therefore, this TENG sensor possesses a great possibility to be utilized in the fields of human health monitoring or human–machine interactions.

CONCLUSIONS

In conclusion, electricity generation based on the dynamic EDL at the hydrogel–dielectric polymer interfaces was demonstrated, and the mechano-to-electrical energy conversion mechanism was systematically discussed. The mechanical deformation of the pyramid-shaped hydrogel resulted in the change of the EDL

area, and then the electrified surfaces of the dielectric polymers induced the alternative current flowing through the external circuits. By adding LiCl salt or EG solvent into the hydrogel, the electrification was suppressed and the output decreased. Nevertheless, the EG additive can promote the antifreeze and anti-dehydration performances of these hydrogel-based devices. Furthermore, we constructed a soft and stretchable self-powered pressure sensor based on dynamic hydrogel–PDMS interfaces. By increasing the roughness of the PDMS surface, the sensitivity reached 1.40 kPa^{-1} in the low pressure range of 31 to 300 Pa. Due to the high sensitivity, softness, and stretchability of the self-powered sensor, its capability in detecting subtle human activities was demonstrated, such as throat movements, vocal cord vibrations, muscle motions, and abdominal breathing.

METHODS

Materials. Herein, acrylamide (AAM), lithium chloride (LiCl), sodium chloride (NaCl), *N,N'*-methylenebis(acrylamide) (MBAA), ammonium persulfate (AP), *N,N,N',N'*-tetramethylethylenediamine (TEMED) were purchased from Sigma-Aldrich. Ethylene glycol (EG) was purchased from Aladdin. Sylgard 184 (PDMS) was used as the elastomer.

Preparation of PAM Hydrogel Arrays. At first, 1.6 g AAM, 0.01 g MBAA, and 0.05 g AP were added to 10 mL deionized water. Then, the suspension was stirred at 750 rpm until drugs were completely dissolved. Next, different concentrations of LiCl or NaCl (0, 0.05, 0.1, 0.5, 1, and 2 M, respectively) were dissolved into the clarified solution above. A 15 min ultrasonic water bath was used to remove the air bubble in the solution. The solution was then poured into a mold ($4 \text{ cm} \times 4 \text{ cm}$) with the pyramid arrays ($4 \text{ mm} \times 4 \text{ mm} \times 3 \text{ mm}$, $7 \text{ pixel} \times 7 \text{ pixel}$) as shown in Figure S1(i). After that, the bubbles existing between the solution and the mold were removed by a needle, and a drop of catalyst TEMED was instilled into the solution. Finally, the solution will be cured within 10 min and the hydrogel arrays were obtained.

Preparation of Vertical Contact-Separation Mode TENG. The structure of the TENG is illustrated in Figure 1a. Two copper films were selected as the parallel-configured electrodes. The polytetrafluoroethylene tape (thickness: $70 \mu\text{m}$, $4 \text{ cm} \times 4 \text{ cm}$) and the hydrogel arrays were attached on the two Cu electrodes to serve as dielectric layers, respectively.

Preparation of Single-Electrode Mode TENG. The PDMS film (The ratio of Sylgard 184 and curing agent is 10:1 by weight) was obtained by spin-coating at first, and then cured at 60 °C for 3 h (Figure S1(ii)). The single-electrode mode TENG was assembled by using the hydrogel arrays as electrode and PDMS as dielectric layer, as shown in Figure 3a.

Characterization and Measurement. A step motor (LinMot E1100) was employed to simulate the mechanical vibration, and the speed (1 m/s) and frequency ($\sim 5 \text{ Hz}$) of the step motor were fixed for all tests. Meanwhile, the output of the TENG were measured by an electrometer Keithley 6517. The force imposed by the motor was recorded by a Mark-10 force gauge. For measuring the output performance of the TENG at low temperature, the TENG was put into a thermostat (GDW-50L, Wuxi Zhongtian Company) and a linear motor was stuck into the thermostat to control the TENG through a feed through hole. The morphology of PDMS film and lyophilized hydrogel were received by field emission scanning electron microscope (Nova 250 SEM, FEI Company). The ESM301/Mark-10 system was used to test the mechanical tensile of the hydrogel and the strain test was fixed at 30 mm/min . The impedance test was proceeded by an electrochemical workstation (CHI660E), and the samples were sandwiched by two stainless steel electrodes for tests.

ASSOCIATED CONTENT

Supporting Information

The Supporting Information is available free of charge at <https://pubs.acs.org/doi/10.1021/acsnano.1c06950>.

Figures S1–S18: sketch map of experimental, output characteristics curve of TENG under different conditions and resistance, the equivalent circuit model of the TENG, the frequency response characteristics of the TENG and sensor, the Q_{sc} of the TENG when using the hydrogel containing different concentrations of NaCl solution, the open-circuit voltage of TENG after dehydration, the impedance chart of the selected PAM hydrogel, output characteristics of the TENG sensor with the PDMS of different thickness, the complete mechanism of the TENG sensor, the mechanical durability and response time characterization of the sensor, tensile stress–strain curves of the selected PAM hydrogel, photos of the TENG sensor being twisted, the output voltage peak value of the sensor measured at different temperatures under 2 KPa, the electrical signals of TENG sensor under different human motion and theoretical analysis of TENG output characteristics (PDF)

Video 1: Process of the TENG sensor monitoring human motor (MP4)

AUTHOR INFORMATION

Corresponding Authors

Xiong Pu – CAS Center for Excellence in Nanoscience, Beijing Key Laboratory of Micro-Nano Energy and Sensor, Beijing Institute of Nanoenergy and Nanosystems, Chinese Academy of Sciences, Beijing 101400, P. R. China; School of Nanoscience and Technology, University of Chinese Academy of Sciences, Beijing 100049, P. R. China; Center on Nanoenergy Research, School of Chemistry and Chemical Engineering, School of Physical Science and Technology, Guangxi University, Nanning 530004, P. R. China; CUSTech Institute of Technology, Wenzhou, Zhejiang 325024, China; orcid.org/0000-0002-1254-8503; Email: puxiong@binn.cas.cn

Zhong Lin Wang – CAS Center for Excellence in Nanoscience, Beijing Key Laboratory of Micro-Nano Energy and Sensor, Beijing Institute of Nanoenergy and Nanosystems, Chinese Academy of Sciences, Beijing 101400, P. R. China; School of Nanoscience and Technology, University of Chinese Academy of Sciences, Beijing 100049, P. R. China; Center on Nanoenergy Research, School of Chemistry and Chemical Engineering, School of Physical Science and Technology, Guangxi University, Nanning 530004, P. R. China; CUSTech Institute of Technology, Wenzhou, Zhejiang 325024, China; School of Material Science and Engineering, Georgia Institute of Technology, Atlanta, Georgia 30332-0245, United States; orcid.org/0000-0002-5530-0380; Email: zlwang@gatech.edu

Authors

Luyao Jia – CAS Center for Excellence in Nanoscience, Beijing Key Laboratory of Micro-Nano Energy and Sensor, Beijing Institute of Nanoenergy and Nanosystems, Chinese Academy of Sciences, Beijing 101400, P. R. China; School of Nanoscience and Technology, University of Chinese Academy of Sciences, Beijing 100049, P. R. China

Zi Hao Guo – CAS Center for Excellence in Nanoscience, Beijing Key Laboratory of Micro-Nano Energy and Sensor, Beijing Institute of Nanoenergy and Nanosystems, Chinese Academy of Sciences, Beijing 101400, P. R. China; School of Nanoscience and Technology, University of Chinese Academy of Sciences, Beijing 100049, P. R. China

Longwei Li – CAS Center for Excellence in Nanoscience, Beijing Key Laboratory of Micro-Nano Energy and Sensor, Beijing Institute of Nanoenergy and Nanosystems, Chinese Academy of Sciences, Beijing 101400, P. R. China; School of Nanoscience and Technology, University of Chinese Academy of Sciences, Beijing 100049, P. R. China

Chongxiang Pan – CAS Center for Excellence in Nanoscience, Beijing Key Laboratory of Micro-Nano Energy and Sensor, Beijing Institute of Nanoenergy and Nanosystems, Chinese Academy of Sciences, Beijing 101400, P. R. China; Center on Nanoenergy Research, School of Chemistry and Chemical Engineering, School of Physical Science and Technology, Guangxi University, Nanning 530004, P. R. China

Panpan Zhang – CAS Center for Excellence in Nanoscience, Beijing Key Laboratory of Micro-Nano Energy and Sensor, Beijing Institute of Nanoenergy and Nanosystems, Chinese Academy of Sciences, Beijing 101400, P. R. China

Fan Xu – CAS Center for Excellence in Nanoscience, Beijing Key Laboratory of Micro-Nano Energy and Sensor, Beijing Institute of Nanoenergy and Nanosystems, Chinese Academy of Sciences, Beijing 101400, P. R. China; School of Nanoscience and Technology, University of Chinese Academy of Sciences, Beijing 100049, P. R. China

Complete contact information is available at:

<https://pubs.acs.org/10.1021/acsnano.1c06950>

Author Contributions

X.P., Z.L.W., and L.J. conceived the project and designed the experiments. L.J. and Z.H.G. contributed to sample preparation. L.J. and Z.H.G. performed the experiments. C.P., L.L., P.Z., and F.X. contributed to data analysis. All authors discussed the results and commented on the manuscript. L.J., X.P., and Z.L.W. wrote the paper with input from all authors.

Funding

National Natural Science Foundation of China (52173274).

Notes

The authors declare no competing financial interest.

ACKNOWLEDGMENTS

The authors thank for the support from National Natural Science Foundation of China (52173274).

REFERENCES

- (1) Parsons, R. Electrical Double-Layer-Recent Experimental and Theoretical Developments. *Chem. Rev.* **1990**, *90*, 813–826.
- (2) Xu, R.; Shen, X.; Ma, X. X.; Yan, C.; Zhang, X. Q.; Chen, X.; Ding, J. F.; Huang, J. Q. Identifying the Critical Anion-Cation Coordination to Regulate the Electric Double Layer for an Efficient Lithium-Metal Anode Interface. *Angew. Chem., Int. Ed.* **2021**, *60*, 4215–4220.
- (3) Liu, K.; Ding, T.; Mo, X.; Chen, Q.; Yang, P.; Li, J.; Xie, W.; Zhou, Y.; Zhou, J. Flexible Microfluidics Nanogenerator Based on the Electrokinetic Conversion. *Nano Energy* **2016**, *30*, 684–690.
- (4) Ong, G. M. C.; Gallegos, A.; Wu, J. Modeling Surface Charge Regulation of Colloidal Particles in Aqueous Solutions. *Langmuir* **2020**, *36*, 11918–11928.
- (5) Wang, Z. L. From Contact-Electrification to Triboelectric Nanogenerators. *Rep. Prog. Phys.* **2021**, *84*, 096502.
- (6) Lin, Z. H.; Cheng, G.; Lin, L.; Lee, S.; Wang, Z. L. Water-Solid Surface Contact Electrification and Its Use for Harvesting Liquid-Wave Energy. *Angew. Chem.* **2013**, *52*, 12545–12549.
- (7) Zhu, G.; Su, Y. J.; Bai, P.; Chen, J.; Jing, Q. S.; Yang, W. Q.; Wang, Z. L. Harvesting Water Wave Energy by Asymmetric Screening of Electrostatic Charges on a Nanostructured Hydrophobic Thin-Film Surface. *ACS Nano* **2014**, *8*, 6031–6037.

- (8) Xu, W.; Zheng, H.; Liu, Y.; Zhou, X.; Zhang, C.; Song, Y.; Deng, X.; Leung, M.; Yang, Z.; Xu, R. X.; Wang, Z. L.; Zeng, X. C.; Wang, Z. A Droplet-Based Electricity Generator with High Instantaneous Power Density. *Nature* **2020**, *578*, 392–396.
- (9) Liu, K.; Yang, P.; Li, S.; Li, J.; Ding, T.; Xue, G.; Chen, Q.; Feng, G.; Zhou, J. Induced Potential in Porous Carbon Films through Water Vapor Absorption. *Angew. Chem., Int. Ed.* **2016**, *55*, 8003–8007.
- (10) Xue, G.; Xu, Y.; Ding, T.; Li, J.; Yin, J.; Fei, W.; Cao, Y.; Yu, J.; Yuan, L.; Gong, L.; Chen, J.; Deng, S.; Zhou, J.; Guo, W. Water-Evaporation-Induced Electricity with Nanostructured Carbon Materials. *Nat. Nanotechnol.* **2017**, *12*, 317–321.
- (11) Cheng, H.; Huang, Y.; Zhao, F.; Yang, C.; Zhang, P.; Jiang, L.; Shi, G.; Qu, L. Spontaneous Power Source in Ambient Air of a Well-Directionally Reduced Graphene Oxide Bulk. *Energy Environ. Sci.* **2018**, *11*, 2839–2845.
- (12) Wang, H.; Sun, Y.; He, T.; Huang, Y.; Cheng, H.; Li, C.; Xie, D.; Yang, P.; Zhang, Y.; Qu, L. Bilayer of Polyelectrolyte Films for Spontaneous Power Generation in Air up to an Integrated 1,000 V Output. *Nat. Nanotechnol.* **2021**, *16*, 811–819.
- (13) Liu, X.; Gao, H.; Ward, J. E.; Liu, X.; Yin, B.; Fu, T.; Chen, J.; Lovley, D. R.; Yao, J. Power Generation from Ambient Humidity Using Protein Nanowires. *Nature* **2020**, *578*, 550–554.
- (14) Zheng, L.; Cheng, G.; Chen, J.; Lin, L.; Wang, J.; Liu, Y.; Li, H.; Wang, Z. L. A Hybridized Power Panel to Simultaneously Generate Electricity from Sunlight, Raindrops, and Wind around the Clock. *Adv. Energy Mater.* **2015**, *5*, 1501152.
- (15) Moon, J. K.; Jeong, J.; Lee, D.; Pak, H. K. Electrical Power Generation by Mechanically Modulating Electrical Double Layers. *Nat. Commun.* **2013**, *4*, 1487.
- (16) Yoon, S. G.; Yang, Y.; Jin, H.; Lee, W. H.; Sohn, A.; Kim, S. W.; Park, J.; Kim, Y. S. A Surface-Functionalized Ionovoltaic Device for Probing Ion-Specific Adsorption at the Solid-Liquid Interface. *Adv. Mater.* **2019**, *31*, No. e1806268.
- (17) Helseth, L. E.; Guo, X. D. Contact Electrification and Energy Harvesting Using Periodically Contacted and Squeezed Water Droplets. *Langmuir* **2015**, *31*, 3269–3276.
- (18) Lin, S.; Xu, L.; Chi Wang, A.; Wang, Z. L. Quantifying Electron-Transfer in Liquid-Solid Contact Electrification and the Formation of Electric Double-Layer. *Nat. Commun.* **2020**, *11*, 399.
- (19) Lin, S.; Chen, X.; Wang, Z. L. The Tribovoltaic Effect and Electron Transfer at a Liquid-Semiconductor Interface. *Nano Energy* **2020**, *76*, 105070.
- (20) Lin, S.; Chen, X.; Wang, Z. L. Contact Electrification at the Liquid-Solid Interface. *Chem. Rev.* **2021**, *1* DOI: 10.1021/acscchemrev.1c00176.
- (21) Yin, J.; Zhang, Z.; Li, X.; Yu, J.; Zhou, J.; Chen, Y.; Guo, W. Waving Potential in Graphene. *Nat. Commun.* **2014**, *5*, 3582.
- (22) Yang, S.; Su, Y.; Xu, Y.; Wu, Q.; Zhang, Y.; Raschke, M. B.; Ren, M.; Chen, Y.; Wang, J.; Guo, W.; Ron Shen, Y.; Tian, C. Mechanism of Electric Power Generation from Ionic Droplet Motion on Polymer Supported Graphene. *J. Am. Chem. Soc.* **2018**, *140*, 13746–13752.
- (23) Yin, J.; Li, X.; Yu, J.; Zhang, Z.; Zhou, J.; Guo, W. Generating Electricity by Moving a Droplet of Ionic Liquid along Graphene. *Nat. Nanotechnol.* **2014**, *9*, 378–83.
- (24) Nie, J.; Ren, Z.; Xu, L.; Lin, S.; Zhan, F.; Chen, X.; Wang, Z. L. Probing Contact-Electrification-Induced Electron and Ion Transfers at a Liquid-Solid Interface. *Adv. Mater.* **2020**, *32*, No. e1905696.
- (25) Lin, S.; Zheng, M.; Wang, Z. L. Detecting the Liquid-Solid Contact Electrification Charges in a Liquid Environment. *J. Phys. Chem. C* **2021**, *125*, 14098–14104.
- (26) Wang, Z. L.; Wang, A. C. On the Origin of Contact-Electrification. *Mater. Today* **2019**, *30*, 34–51.
- (27) Lacks, D. J.; Shinbrot, T. Long-standing and Unresolved Issues in Triboelectric Charging. *Nat. Rev. Chem.* **2019**, *3*, 465–476.
- (28) Lim, K. H.; Sun, Y.; Lim, W. C.; Soh, S. Charging Organic Liquids by Static Charge. *J. Am. Chem. Soc.* **2020**, *142*, 21004–21016.
- (29) Jiang, B.; Long, Y.; Pu, X.; Hu, W.; Wang, Z. L. A Stretchable, Harsh Condition-Resistant and Ambient-Stable Hydrogel and Its Applications in Triboelectric Nanogenerator. *Nano Energy* **2021**, *86*, 106086.
- (30) Yang, L.; Liu, H.; Ding, S.; Wu, J.; Zhang, Y.; Wang, Z.; Wei, L.; Tian, M.; Tao, G. Superabsorbent Fibers for Comfortable Disposable Medical Protective Clothing. *Adv. Fiber Mater.* **2020**, *2*, 140–149.
- (31) Yun, G.; Tang, S.-Y.; Lu, H.; Zhang, S.; Dickey, M. D.; Li, W. Hybrid-Filler Stretchable Conductive Composites: From Fabrication to Application. *Small Sci.* **2021**, *1*, 2000080.
- (32) Bao, R.; Tao, J.; Pan, C.; Wang, Z. L. Piezophototronic Effect in Nanosensors. *Small Sci.* **2021**, *1*, 2000060.
- (33) Zhou, Q.; Lee, K.; Deng, S.; Seo, S.; Xia, F.; Kim, T. Portable Triboelectric Microfluidic System for Self-Powered Sensors towards *in-Situ* Detection. *Nano Energy* **2021**, *85*, 105980.
- (34) Xie, M.; Zhu, M.; Yang, Z.; Okada, S.; Kawamura, S. Flexible Self-Powered Multifunctional Sensor for Stiffness-Tunable Soft Robotic Gripper by Multimaterial 3D Printing. *Nano Energy* **2021**, *79*, 105438.
- (35) Wang, Z. L. Triboelectric Nanogenerators as New Energy Technology for Self-Powered Systems and as Active Mechanical and Chemical Sensors. *ACS Nano* **2013**, *7*, 9533–9557.
- (36) Zhang, R.; Wang, S.; Yeh, M. H.; Pan, C.; Lin, L.; Yu, R.; Zhang, Y.; Zheng, L.; Jiao, Z.; Wang, Z. L. A Streaming Potential/Current-Based Microfluidic Direct Current Generator for Self-Powered Nanosystems. *Adv. Mater.* **2015**, *27*, 6482–6487.
- (37) Moon, J. K.; Song, M. W.; Pak, H. K. Investigation of Surface Charge Density on Solid-Liquid Interfaces by Modulating the Electrical Double Layer. *J. Phys.: Condens. Matter* **2015**, *27*, 194102.
- (38) Zhan, F.; Wang, A. C.; Xu, L.; Lin, S.; Shao, J.; Chen, X.; Wang, Z. L. Electron Transfer as a Liquid Droplet Contacting a Polymer Surface. *ACS Nano* **2020**, *14*, 17565–17573.
- (39) Loh, Z. H.; Doumy, G.; Arnold, C.; Kjellsson, L.; Southworth, S. H.; Al Haddad, A.; Kumagai, Y.; Tu, M. F.; Ho, P. J.; March, A. M.; Schaller, R. D.; Bin Mohd Yusof, M. S.; Debnath, T.; Simon, M.; Welsch, R.; Inhester, L.; Khalili, K.; Nanda, K.; Krylov, A. I.; Moeller, S.; et al. Observation of the fastest chemical processes in the radiolysis of water. *Science* **2020**, *367*, 179–182.
- (40) Zhang, P.; Chen, Y.; Guo, Z. H.; Guo, W.; Pu, X.; Wang, Z. L. Stretchable, Transparent, and Thermally Stable Triboelectric Nanogenerators Based on Solvent-Free Ion-Conducting Elastomer Electrodes. *Adv. Funct. Mater.* **2020**, *30*, 1909252.
- (41) Pu, X.; Liu, M.; Chen, X.; Sun, J.; Du, C.; Zhang, Y.; Zhai, J.; Hu, W.; Wang, Z. L. Ultrastretchable, Transparent Triboelectric Nanogenerator as Electronic Skin for Biomechanical Energy Harvesting and Tactile Sensing. *Sci. Adv.* **2017**, *3*, No. e1700015.
- (42) Shimoaka, T.; Hasegawa, T. Molecular Structural Analysis of Hydrated Ethylene Glycol Accounting for the Antifreeze Effect by Using Infrared Attenuated Total Reflection Spectroscopy. *J. Mol. Liq.* **2016**, *223*, 621–627.
- (43) Cordray, D. R.; Kaplan, L. R.; Woyciesjes, P. M.; Kozak, T. F. Solid-Liquid Phase Diagram for Ethylene Glycol Plus Water. *Fluid Phase Equilib.* **1996**, *117*, 146–152.
- (44) Ouyang, H.; Tian, J.; Sun, G.; Zou, Y.; Liu, Z.; Li, H.; Zhao, L.; Shi, B.; Fan, Y.; Fan, Y.; Wang, Z. L.; Li, Z. Self-Powered Pulse Sensor for Antidiastole of Cardiovascular Disease. *Adv. Mater.* **2017**, *29*, 1703456.
- (45) Chen, S.; Wu, N.; Lin, S.; Duan, J.; Xu, Z.; Pan, Y.; Zhang, H.; Xu, Z.; Huang, L.; Hu, B.; Zhou, J. Hierarchical Elastomer Tuned Self-Powered Pressure Sensor for Wearable Multifunctional Cardiovascular Electronics. *Nano Energy* **2020**, *70*, 104460.
- (46) Jing, X.; Li, H.; Mi, H. Y.; Feng, P. Y.; Tao, X.; Liu, Y.; Liu, C.; Shen, C. Enhancing the Performance of a Stretchable and Transparent Triboelectric Nanogenerator by Optimizing the Hydrogel Ionic Electrode Property. *ACS Appl. Mater. Interfaces* **2020**, *12*, 23474–23483.
- (47) Jing, X.; Li, H.; Mi, H. Y.; Feng, P. Y.; Tao, X.; Liu, Y.; Liu, C.; Shen, C. A Flexible Semitransparent Dual-Electrode Hydrogel Based Triboelectric Nanogenerator with Tough Interfacial Bonding and High Energy Output. *J. Mater. Chem. C* **2020**, *8*, 5752–5760.
- (48) Bai, N.; Wang, L.; Wang, Q.; Deng, J.; Wang, Y.; Lu, P.; Huang, J.; Li, G.; Zhang, Y.; Yang, J.; Xie, K.; Zhao, X.; Guo, C. F. Graded

Intrafillable Architecture-Based Iontronic Pressure Sensor with Ultra-Broad-Range High Sensitivity. *Nat. Commun.* **2020**, *11*, 209.

(49) Nie, B.; Li, R.; Cao, J.; Brandt, J. D.; Pan, T. Flexible Transparent Iontronic Film for Interfacial Capacitive Pressure Sensing. *Adv. Mater.* **2015**, *27*, 6055–6062.